6.5 TURBULENT FLOWS

E. Bodenschatz, M. Emran, B. Hejazi, A. Krekhov, C. Küchler, A. Landeta, J. Moláček, P. Reiter, O. Shishkina, A. Teimurazov, S. Weiss, X. Zhang, L. Zwirner

G. Ahlers (University of California, Santa Barbara), G. P. Bewley (Cornell University), E. S. C. Ching (University of Hong Kong), R. E. Ecke (Los Alamos National Laboratory and University of Washington), X. He (Harbin Institute of Technology), D. P. M. van Gils, D. Krug, D. Lohse (University of Twente), P. Frick, R. Stepanov (Institute of Continuous Media Mechanics RAS)

Turbulent flows are omnipresent. Their role in geophysical and astrophysical systems and many engineering applications can hardly be overestimated. We investigate turbulence experimentally, theoretically, and numerically and focus in our studies on large-Reynolds-number flows and turbulent thermal convection.

6.5.1 *Turbulent Flows at High Reynolds Numbers*

(C. Küchler) Turbulent flows at large Reynolds numbers R_λ, where viscosity ν plays only a minor role over a wide range of spatial and temporal scales, exhibit a remarkable level of self-organisation, which largely remains to be understood at a fundamental level with wide ranging applications, among others, to atmospheric dynamics. Of particular importance are scales r much smaller than the turbulence excitation scale L, but larger than the viscous length scale η. The statistical properties of motion are expected to be dominated by inertia and to be universal for small ν. Using the MPI DS Variable Density Turbulence Tunnel (VDTT), we have shown that the statistics of these inertial scales approach an asymptotic shape when increasing R_λ. This shape is different from the classical predictions [1], which postulates simple power laws as a function of scale. This is illustrated in Fig. 6.14 for the local scaling exponent of the second-order velocity increment statistics, i.e. $\zeta_2 = \partial \log\langle u(x+r) - u(x)\rangle / \partial \log r$. We have collected evidence that the time-dependence of the decaying flow causes this R_λ-independent breaking of scale invariance. In the past, such effects were attributed to finite R_λ and predicted to fade when R_λ is large enough. Our results indicate that this may only be true under the highly idealised conditions of homogeneous, isotropic and statistically stationary turbulence, which do not apply in real flows even in the conceptually simple configuration of a wind tunnel, where (time-dependent) large-scale effects appear to influence small-scale statistics even when R_λ is extremely large.

In Fig. 6.14 a small knee is visible in the experimental data around $r/\eta = 100$. In this region the statistics are dominated by the bottleneck effect leading to a small excess of energy at the scales small enough that viscosity begins to matter [2]. This excess energy has been shown to diminish with increasing R_λ in numerical simulations [3]. Using the flexible parameter space of the VDTT, we have corrected the non-

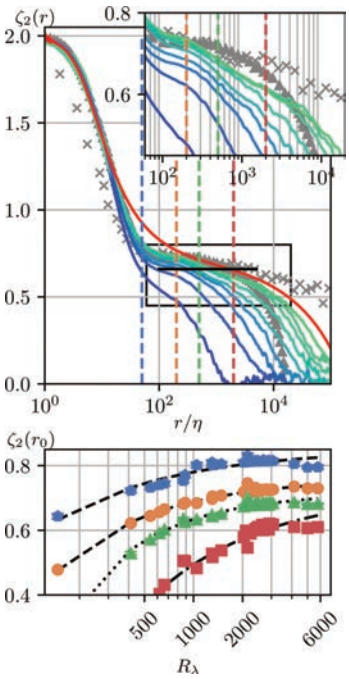

Figure 6.14: Top: Local scaling exponent of the second order velocity increments as a function of r normalised by the viscous length scale η. Colors indicate the Reynolds number from 147 (blue) to 5885 (green). The curves begin to collapse starting around $\mathrm{Re} \approx 2000$. A model accounting for the decay of turbulent kinetic energy (red) follows the data better than a single inertial range scaling exponent (black line). Bottom: Values of ζ_2 evaluated at specific r/η indicated by the dashed lines in the top figure (blue to red: $r_0/\eta = 50, 200, 500, 2000$). Note that the curves approach different asymptotes, i.e. scale-invariance is not found.

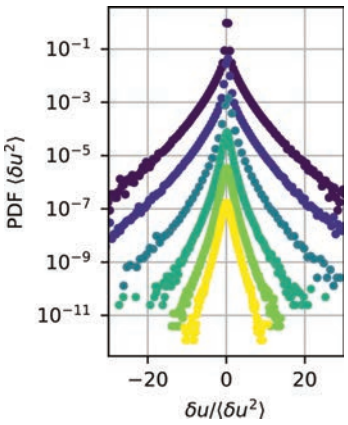

Figure 6.15: Normalised PDFs of the velocity increment $\delta u = u(t+\tau) - u(t)$ at $R_\lambda \approx 5500$. Curves are incrementally shifted for clarity. Uppermost curve: acceleration. Other curves: $\tau = 0.15\tau_\eta, 0.46\tau_\eta, 1.0\tau_\eta, 2.4\tau_\eta, 5.6\tau_\eta$ (yellow).

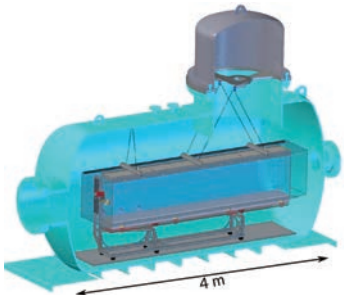

Figure 6.16: Schematic of the U-Boot with our current large aspect rectangular cell inside.

constant frequency response of our flow sensors to measure this subtle effect. We find good agreement between the numerical simulations and the experiment at low R_λ and show that the reduction of the effect continues up to at least $R_\lambda = 3500$, beyond what can been explored numerically. A defining feature of turbulent flows is their efficiency to mix and transport within a fluid. This is most intuitively described by following a fluid element, e.g. by seeding the flow with light particles and tracking their position at high frequencies. This extremely demanding technique has been recently implemented in the VDTT. Using this setup we have measured the highly intermittent accelerations in turbulence at unprecedented Reynolds numbers. Fig. 6.15 shows the acceleration statistics and velocity increment statistics up to $5.6\tau_\eta$ at $R_\lambda \approx 5500$ - more than two times higher than all previous measurements. The heavy-tail nature of the PDFs is clearly visible and we find consistency with earlier experiments at lower Reynolds number (e.g. Refs. [4, 5, 6]). Future studies will investigate the normalised acceleration variance a_0 testing a long-standing scaling prediction [7, 8] at unprecedented Reynolds numbers.

6.5.2 *Turbulent and multiphase convection*

(A. Krekhov, O. Shishkina, S. Weiss) Thermal convection is one of the most important heat transport mechanism and drives large scale turbulent flows, for instance in many geo- and astrophysical systems. We study convection experimentally and theoretically using the Rayleigh–Bénard (RB) setup [9], where a fluid layer of height L, is confined by a warm plate from below and a cold one from above. The dimensionless Rayleigh number (Ra) represents the strength of the thermal driving in this system, and is directly proportional to L^3 and the maximal temperature difference in the system. Our research focuses on different aspects of convection, such as convection at very large thermal driving (large Ra) [10, 11, 12, 13]. We also consider the effect of rotation [14, 15, 16, 17], or of the roughness of the heated and cooled surfaces [18, 19], or of a phase transition in the fluid [20], and other aspects.

The largest convection cells are used in the "U-Boot of Göttingen", which is a 4 m long pressure vessel filled with Sulfur hexafluoride (SF_6) and pressurized up to 19 bar. Using compressed gases allows to change fluid properties and thus the relevant dimensionless control parameters over a very large range. Furthermore, SF_6 is a very dense gas, and thus well suited to achieve very large Ra ($Ra \propto \varrho^2$). With this apparatus Ra of up to 2×10^{15} can be reached and the transition to the "ultimate state" has been probed in the past [12, 13]. We currently investigate the large scale flow structure in thermal convection using a 3.50 m long and 70 cm large aspect ratio convection cell inside the U-Boot.

In turbulent RB convection, the flow in boundary layers exhibits strong fluctuations. Furthermore, the time-averaged large-scale circulating velocity vanishes far away from the top and bottom plates, and the motion arises from buoyancy. We have derived the full set of boundary layer equations for a RB flow, taking into account all the above effects. The solutions of these boundary layer equations give the RB flow field

profiles [21, 22]. We further study the global structure of RB flow, in particular the role of the thermal plume impacting and ejecting zones [23]. The influence on the temperature- and pressure-dependence of the fluid properties, i.e. the so-called non-Oberbeck–Boussinesq effects, have been investigated as well [24, 25]. In particular, we have studied convection in cold water and derived the way to accurately predict the bulk temperature [25].

One of our main focus is to investigate the effect of rotation on the flow field and the heat transport, a topic particularly relevant for geo- and astrophysics. For this we conduct experiments using our $L = 2.20\,\mathrm{m}$ high convection cell inside the U-Boot, in order to achieve very large thermal driving. One of our main finding [14] was the existence of the *boundary zonal flow – BZF* close to the sidewall of the cylindrical cell under rotation. This flow is characterised by a positive averaged azimuthal velocity, in contrast to a negative velocity close to the radial center, as well as periodically alternating warm (upflow) and cold (downflow) regions. These regions furthermore drift in retrograde direction. The region close to the sidewall, where these flow features are observed, shrinks with increasing rotation rate, but still remains to be very important in heat transport in the system, see [14, 15, 16, 17].

The large-scale circulation (LSC) of fluid is one of the main concepts in turbulent thermal convection as it is known to be important in global heat and mass transport in the system. In turbulent RB convection in slender containers, the LSC is formed of several dynamically changing convective rolls that are stacked on top of each other. We have revealed that the mechanism which causes the twisting and breaking of a single-roll LSC into multiple rolls is the elliptical instability [26], see Fig. 6.18.

In contrast to the situation in slender RB containers [26], the heat and momentum transport in RB convection in wide cells, represented by the Nusselt and Reynolds numbers, is always weaker (stronger) for larger (smaller) number of the rolls in the LSC structure [27]. For exactly the same values of the control parameters, RB flow can take different statistically stationary turbulent states, with different transport properties. What state the system takes depends on the initial conditions. In the case of wide containers, the state in determined by the aspect ratios of particular rolls of elliptical shape, for which we have derived the bounds [27].

Many natural and industrial turbulent flows are subjected to time-dependent boundary conditions. We have studied how the time periodic modulation in the temperature boundary condition [28] or imposed travelling thermal waves [29] can influence heat transport (Nusselt number) and formation of zonal flows. In another ongoing project we investigate the heat transport across a sheared thermally unstable boundary layer. There, the hot plate is located in a wind tunnel, so that advection close to the plate surface is caused both by buoyancy and a shear instability. We measure velocities above the plate and the heat flux from the plate as a function of the flow speed and the buoyancy. With this we probe the transition from the regime of natural convection, where buoyancy dominates over the shear forces to the regime of forced convection, where buoyancy can be neglected (see Fig. 6.19).

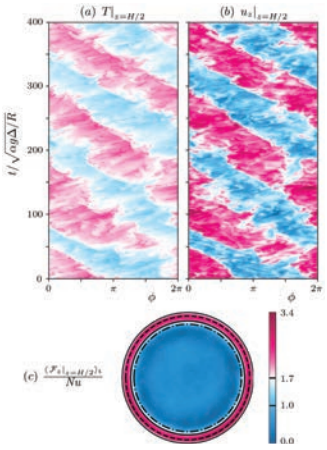

Figure 6.17: Rotational Rayleigh–Bénard convection, for $Ra = 10^9$ and inversed Rossby number $1/Ro = 10$ at the mid height of a tall cylindrical cell of the aspect ratio $\Gamma \equiv D/H = 1/2$: (a,b) angle-time plots of (a) the temperature and (b) the vertical velocity near the sidewall; (c) normalized time-averaged vertical heat flux. Adapted from [14].

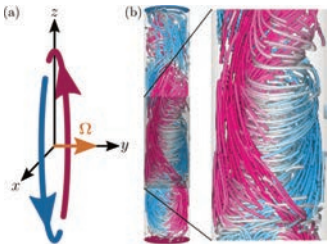

Figure 6.18: (a) Sketch of the primary elliptical LSC, showing the vorticity of the single-roll mode. (b) A snapshot illustrating a strong azimuthal motion, due to the elliptical instability (pink for upward and blue for downward flows). Adapted from [26].

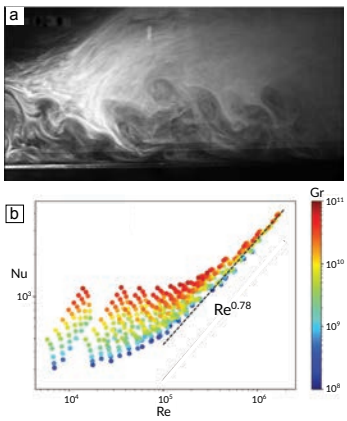

Figure 6.19: (a): Snapshot of the smoke-seeded shear flow over a flat plate heated. (b): Heat transport as a function of the Reynolds number of the incoming flow (x-axis) and the thermal driving (Grashof number *Gr*, color code).

We acknowledge the Max Planck Center for Complex Fluid Dynamics and also the financial support from the Deutsche Forschungsgemeinschaft (DFG): Priority Program (SPP) 1881 "Turbulent Superstructures" and the DFG grants We 5011/4, Sh 405/4, Sh 405/7, Sh 405/8, Sh 405/10, Sh 405/12 and Sh 405/16 as well as Leibniz Supercomputing Centre (LRZ) for providing computer time.

Apart from the classical RB flow configuration we also studied horizontal convection [30, 31], where the heating and cooling are applied to the same horizontal surface of the fluid layer, vertical convection [32], where the fluid is confined between two vertical surfaces of different temperatures, and inclined convection [33, 34], i.e., a mixture of RB and vertical convection.

Finally we should also mention our studies of another omnipresent phenomenon in many geo- and astrophysical convective flows, i.e. internally heated convection, which is a convective fluid motion driven by the internal heat generation. An important question in these studies is how the mean temperature and the global flow strength depend on the internal heating rate and the operating fluid. Recently we have offered a theory to address this question [35]; the results of the theory agree well with direct numerical simulations.

[1] A. N. Kolmogorov, Dokl. Akad. Nauk SSSR **30**, 229 (1941)
[2] G. Falkovich, Phys. Fluids **6**, 1411 (1994)
[3] D. Donzis et al., J. Fluid Mech. **657**, 171 (2010)
[4] E. Bodenschatz et al., Rev. Sci. Inst., **85**, 093908 (2014)
[5] C. Küchler et al., J. Stat. Phys., **175**, 617 (2019)
[6] A. La Porta et al., Nature **409**, 1017 (2001)
[7] W. Heisenberg, Z. Phys. **124**, 628 (1948)
[8] A. M. Yaglom, C. R. Acad. URSS **67**, 795 (1949)
[9] G. Ahlers et al., Rev. Mod. Phys. **81**, 503 (2009)
[10] X. He et al., Phys. Rev. Lett. **108**, 024502 (2012)
[11] G. Ahlers et al., J. Fluid Mech. **758**, 436 (2014)
[12] X. He et al., Phys. Rev. Lett. **124**, 229402 (2020)
[13] X. He et al., Theor. Appl. Mechanics Lett. **11**, 100237 (2021)
[14] X. Zhang et al., Phys. Rev. Lett. **124**, 084505 (2020)
[15] O. Shishkina, J. Fluid Mech. **898**, F1 (2020)
[16] M. Wedi et al., J. Fluid Mech., **912**, A30 (2021)
[17] X. Zhang et al., J. Fluid Mech. **915**, A62 (2021)
[18] X. Zhu et al., J. Fluid Mech. **869**, R4 (2019)
[19] M. Emran, O. Shishkina, J. Fluid Mech. **882**, A3 (2020)
[20] P. Prabhakaran et al., J. Stat. Phys. **175**, 598 (2019)
[21] E. Ching et al., Phys. Rev. Research **1**, 033037 (2019)
[22] N. C. Tai et al., Phys. Rev. Fluids **6**, 033501 (2021)
[23] P. Reiter et al., Europhys. Lett. **134**, 34002 (2021)
[24] H. Yik et al., Phys. Rev. Fluids **5**, 103502 (2020)
[25] Q. Wang et al., Phys. Rev. Fluids **6**, 063502 (2021)
[26] L. Zwirner et al., Phys. Rev. Lett. **125**, 054502 (2020)
[27] Q. Wang et al., Phys. Rev. Lett. **125**, 074501 (2020)
[28] R. Yang et al., Phys. Rev. Lett. **125**, 154502 (2020)
[29] P. Reiter et al., J. Fluid Mech. **913**, A13 (2021)
[30] P. Reiter, O. Shishkina, J. Fluid Mech. **892**, R1 (2020)
[31] B. Yan et al., J. Fluid Mech. **915**, R5 (2021)
[32] Q. Wang et al., J. Fluid Mech. **917**, A6 (2021)
[33] L. Zwirner et al., J. Fluid Mech. **884**, A18 (2020)
[34] A. Teimurazov et al., Europhys. Lett. **134**, 34001 (2021)
[35] Q. Wang et al., Geophys. Res. Lett. **48**, 4 (2021)